J. Biochem. 128, 687–694 (2000)

Solution Structure of Myosin-ADP-MgFn Ternary Complex by Fluorescent Probes and Small-Angle Synchrotron X-Ray Scattering[1]

Shinsaku Maruta,*[2] Tomoki Aihara,* Yasuo Uyehara,* Kazuaki Homma,* Yasunobu Sugimoto,† and Katsuzo Wakabayashi†

Department of Bioengineering, Faculty of Engineering, Soka University, Hachioji, Tokyo 192-8577; and †Department of Biophysical Engineering, Faculty of Engineering Science, Osaka University, Toyonaka, Osaka 560-8531

Received May 31, 2000; accepted August 9, 2000

In the presence of excess amounts of fluorine, a physiological divalent cation, magnesium (Mg^{2+}), forms a novel phosphate analogue, magnesium fluoride (MgFn). Park *et al.* [*Biochim. Biophys. Acta* 1430, 127–140 (1999)] previously demonstrated that MgADP·MgFn forms a complex with myosin subfragment-1 (S-1), and the S-1·ADP·MgFn ternary complex mimics a transient state in the activity cycle of ATPase. In the present study, localized conformations in the regions of highly reactive cysteine and lysine residues, Cys 707 (SH1), Cys 697 (SH2), and Lys 83 (RLR), which change their conformations markedly during ATP hydrolysis, were studied using fluorescent probes and chemical modification. The global shape of the complex was also studied using small angle X-ray solution scattering and compared it with other previously reported myosin·ADP·fluorometal ternary complexes. The results suggest that the overall conformation and localized functional regions of the complex are quite similar to those in the presence of ATP, indicating that the complex mimics the M^{**}·ADP·P_i steady state.

Key words: energy transduction, fluorescent probe, myosin ATPase, transition state complex, X-ray scattering.

Recent crystallographic studies of the heads of skeletal muscle myosin (*1*) and the motor domain of *Dictyostelium* myosin (*2*) have shown the exact structure of the ATP and actin binding sites. A possible molecular model of cross-bridge cycling for muscle contraction was proposed based on the structure of S-1, determined by Rayment *et al.* (*3*). However, the mechanistic details at the molecular level, *i.e.*, how the chemical energy of ATP is converted to energy for the contractile machinery, remain obscure. Several biochemical and physical studies have indicated that the myosin head changes its global conformation and its localized flexible region in a series of steps constituting the ATPase cycle. The conformational changes in the localized regions are reflected by changes in the intrinsic tryptophan fluorescence (*4*), reactivity to chemical modification of several specific amino acid residues SH1, SH2 (*5–7*), and a reactive lysine residue (*8*, *9*). The overall morphological changes of the myosin head during ATP hydrolysis were first identified by small-angle X-ray scattering (*10*). During the contractile cycle, myosin forms a series of intermediates that are directly related to such conformational changes of the myosin head. The study of sequential conformational changes is very important for understanding the mechanisms of energy transduction. However, the intermediates have only limited lifetimes, and it is difficult to isolate each ATPase reaction intermediate for biochemical and biophysical analysis. Therefore, stable analogues corresponding to these species are useful for analyzing their structures.

Recent studies have demonstrated that the phosphate analogues of fluorometals, aluminum fluoride (AlF_4^-), beryllium fluoride (BeFn), scandium fluoride (ScFn), and gallium fluoride (GaFn), form stable ternary complexes, *e.g.*, myosin·ADP·AlF_4^- (*11–13*) myosin·ADP·BeFn (*11–14*), myosin·ADP·ScFn (*15*), and myosin·ADP·GaFn (*16*). Differences in the interaction with actin and localized conformation of these complexes suggest that each complex mimics distinct reaction intermediates in the myosin ATPase cycle (*12*). Moreover, recent crystallographic studies (*2*, *17*) have identified differences between ternary complexes (AlF_4^-, BeFn, V_i) in the conformation of the COOH-terminal segment of the truncated myosin head from *Dictyostelium discoideum* myosin II (S-1Dc). X-ray solution scattering measurement is a useful method for the directly detection of large-scale changes in molecular structure in solution during dynamic functioning under physiological conditions. Wakabayashi and colleagues (*10*, *18*) succeeded in observing the compact or rounded configuration of S-1 in the presence of ATP and $S1^{**}$·ADP·P_i analogue (AlF_4^-, BeFn, and V_i) complexes and demonstrated that the morphology is different from that of S-1 in the absence of nucleotide.

Recently, Park *et al.* (*19*) demonstrated that a new phosphate analogue, magnesium fluoride (MgFn), also forms a

[1] This work was supported by Grants-in-Aid for Scientific Research C (11680667) from the Ministry of Education, Science, Sports and Culture of Japan.

[2] To whom correspondence should be addressed. Fax: +81-426-91-9312, Phone: +81-426-91-9443, E-mail: shinsaku@t.soka.ac.jp

Abbreviations: ABDF, 4-fluoro-7-sulfamoylbenzofurazan; AlF_4^-, aluminum fluoride; BeFn, beryllium fluoride; DTT, dithiothreitol; GaFn, gallium fluoride; MIANS, 2-(4′-maleimidylanilino)naphthalene-6-sulfonic acid; PP_i, pyrophosphate; Prodan, 6-propionyl-2-(dimethylamino)naphthalene; RLR, highly reactive lysine residue; S-1, myosin subfragment-1; S-1Dc, myosin head from *Dictyostelium discoideum* myosin II; ScFn, scandium fluoride; TNBS, trinitrobenzene sulfonate; V_i, vanadate.

stable ternary complex with myosin and ADP. Furthermore, the CD spectra, intrinsic tryptophan enhancement, and acrylamide quenching of Trp510 of the myosin·ADP·MgFn complex suggest that the complex resembles ATPase transients that occur during ATP hydrolysis before phosphate release. In the present study, we examined the localized and global structures of the S-1·ADP·MgFn complex to characterize the structure of the new complex, and compared it with those of other complexes previously reported. The conformations at the localized flexible regions (SH1, SH2, and RLR) of the S-1·ADP·MgFn complex were analyzed using chemical-modification fluorescence labeling. These regions may play an important role in energy transduction, especially the SH1-SH2 region that is considered as an energy transduction loop through which intersite communication between the ATP and actin binding sites is transmitted. In fact, the region markedly changes its conformation along the ATPase kinetic pathway. We also employed small-angle synchrotron X-ray scattering to study the global conformation of the new complex.

The experimental data in the present study demonstrate that the S-1·ADP·MgFn complex mimics the M**·ADP·P_i steady-state in the ATPase cycle. We also discuss the possible order of alignment of the ternary complexes at different transient states, which mimic each other along the ATPase cycle.

MATERIALS AND METHODS

Proteins and Chemicals—Myosin was prepared from chicken breast muscles by the method of Perry (*20*). The isolated myosin was then digested with α-chymotrypsin to obtain subfragment-1 (S-1), as described by Weeds and Taylor (*21*). MIANS, ABDF and prodan were purchased from Molecular Probes (Eugene, OR).

ABDF Labeling of S-1—Fluorescent labeling of S-1 with ABDF was carried out by reacting 10 μM S-1 and 30 mM ABDF in the presence of 20 mM cacodylate (pH 7.3) and 30 mM KCl for 1 h at 4°C in total darkness. The reaction was stopped by adding dithiothreitol (DTT) to a final concentration of 20 mM. The labeled S-1 was then passed through a Sephadex G-50 column equilibrated with 30 mM Tris-HCl (pH 8.0) and 120 mM NaCl. The stoichiometry of the incorporated ABD group/S-1 was determined from the absorption spectrum using an extinction coefficient of 6,000 M^{-1} cm^{-1} at 378 nm. Quantitative analysis of ABD-S-1 was made by staining with Coomassie Brilliant Blue plus protein assay (PIERCE).

MIANS Labeling of S-1—Initially, S-1 was blocked by reacting 40 μM S-1 with 160 μM 2,4-dinitro-1-fluorobenzene (FDNB) in the presence of 0.5 M KCl, 50 mM Tris-HCl (pH 7.8), 2 mM $MgCl_2$, and 1 mM ADP for 20 min on ice. The blocked S-1 was then passed through a Sephadex G-50 column equilibrated with 30 mM Tris-HCl (pH 7.5) and 120 mM NaCl. In the next step, the blocked S-1 (20 μM) was reacted with 26 μM MIANS in the presence of 30 mM KCl, 25 mM Tris-HCl (pH 7.8), 2.5 mM $MgCl_2$, and 1 mM ADP for 30 min at 4°C in total darkness; the reaction was terminated by the addition of 10 mM DTT. The DNP group was then removed from S-1 by further overnight incubation with 10 mM DTT at 4°C in total darkness. MIANS-S-1 was subsequently passed through a Sephadex G-50 column equilibrated with 30 mM Tris-HCl (pH 8.0) and 120 mM NaCl. The stoichiometry of the incorporated MIANS groups/S-1 was determined from differences in the absorption spectra of MIANS-S-1 and unlabeled S-1 using an extinction coefficient of 1.7×10^4 M^{-1} cm^{-1} at 318 nm. The concentration of MIANS-S-1 was determined using Coomassie plus protein assay reagent (PIERCE).

Fluorescence Measurements—Fluorescence measurements for MIANS labeled S-1 and ABDF labeled S-1 were performed at 25°C with an RF-5000 Spectrofluorometer (Shimadzu). Uncorrected fluorescence emission spectra of prodan·S-1·ADP·P_i analogue complexes were recorded at 25°C with a Hitachi fluorescence spectrophotometer (model F-2500).

Trinitrophenylation of S-1·ADP·P_i Analogue Complexes—S-1 (12 μM) was reacted with 0.25 mM trinitrobenzene-sulfonate at 25°C in 100 mM imidazole-HCl (pH 7.0), 0.5 M KCl, 5 mM $MgCl_2$ (or 5 mM $CaCl_2$) in the presence of 2 mM ATP, 2 mM ADP, or 2 mM ADP + 1 mM BeFn (AlF_4^- or ScFn). The time course of trinitrophenylation was monitored at 345 nm using a spectrophotometer equipped with a temperature-controlled cell (Shimadzu UV 2200).

X-Ray Solution Scattering—X-ray solution scattering experiments were performed at 19°C with a small-angle diffractometer, using synchrotron radiation at the Photon Factory (Tsukuba) according to the method of Wakabayashi *et al.* (*10*). The scattering curves from S-1 samples were recorded with a one-dimensional position sensitive detector up to the scattering length $S = 0.02$ Å^{-1} [$S = 2\sin\theta/\lambda$ where 2θ is the scattering angle and λ is the wavelength of the X-rays (1.54 Å)] at a camera length of 2.33 m. The protein concentration used varied from 3 to 12 mg/ml. Each sample was centrifuged just before the X-ray experiments to remove any aggregates. As controls, S-1 samples without nucleotide and in the presence of MgATP were measured. The apparent radius of gyration (R_g) was calculated from the slope of the linear region in the Guinier plot {log[I (S)] *vs.* S^2 (superscript)} of the scattering intensity data. The true R_g value was estimated by extrapolating the calculated values to zero protein concentration.

RESULTS

Conformation of S-1·ADP·MgFn Complex at Localized Flexible Regions—The region of the reactive cysteine residues, SH1 (Cys-707) and SH2 (Cys-697), is highly flexible and changes its conformation upon the binding of ATP and actin (*22–24*). The sequence of transient intermediate along the ATPase kinetic pathway may be reflected in the conformational changes in this region. Hiratsuka (*25, 26*) showed that conformational changes at the reactive thiols associated with ATP hydrolysis could be monitored by fluorescent probes, ABDF and MIANS, labeled at SH1 and SH2, respectively. We labeled the reactive thiols of S-1 with a fluorescent probe using the method of Hiratsuka (*25, 26*) and monitored changes in the fluorescence intensity of the probe bound to the residue, associated with the formation of the S-1·ADP·MgFn ternary complex.

Figure 2 shows the time course of the fluorescence changes in S-1 labeled by ABDF at SH1 (ABD-S-1) upon the addition of ligands. Upon the addition of ATP, the fluorescence intensity of ABD-S-1 at 500 nm increased by 110% due to the formation of a steady-state. After hydrolysis of all the added ATP, the fluorescence intensity decreased to a

level identical to that seen in the presence of ADP. In the presence of ADP and MgFn, the fluorescence intensity increased, indicating the formation of a ternary complex. The maximum intensity attained was that seen in the presence of ATP. The time course of the fluorescence increase due to the formation of ABD-S-1·ADP·MgFn was biphasic, indicating the formation of a complex passing through two steps. This is consistent with the data of Park *et al.* (*19*) suggesting that the formation of the inhibitory complex comprises at least two steps. The emission maximum also blue shifted from 497 to 494 nm due to the formation of ABD-S-1·ADP·MgFn (Fig. 2 inset), coinciding with that in the presence of ATP as reported by Hiratsuka (*25*). Other ABD-S-1·ADP·fluorometal complexes showed the same spectral changes as ABD-S-1·ADP·MgFn. These results suggest that SH1 moves to the more hydrophobic protein interior associated with the formation of the S-1·ADP·MgFn complex as occurs during steady-state ATP hydrolysis.

The conformational change at SH2 caused by the formation of the S-1·ADP·MgFn complex was also monitored by the fluorescence of MIANS-S-1. As shown in Fig. 3, when ATP was added to MIANS-S-1, the fluorescence intensity decreased by 32% due to the formation of a steady-state, consistent with the previous results reported by Hiratsuka (*25*). After hydrolysis of all the added ATP to ADP, the fluorescence intensity at 420 nm increased to a level identical to that seen in the presence of ADP. Upon the addition of MgFn, the fluorescence intensity decreased to the same level as that seen in the presence of ATP due to the formation of the S-1·ADP·MgFn ternary complex. Formation of the MIANS-S-1·ADP·MgFn complex also produced a red shift from 423 to 429 nm in the emission maximum (Fig. 3 inset), coinciding with that seen in the presence of ATP. Hiratsuka clearly demonstrated that the fluorescent probe MIANS sensitively changes its fluorescence intensity and emission maximum depending on hydrophobic strength, showing increasing fluorescence intensity and a blue-shift in more hydrophobic environments (*26*). These results suggest that the formation of the S-1·ADP·MgFn complex results in the movement of SH2 towards a less hydrophobic environment, similar to that seen in the presence of ATP.

The myosin head also contains one highly reactive lysine residue (RLR; Lys 83), which is rapidly and stoichiometrically modified by TNBS (*27*). Trinitrophenylation of RLR markedly changes the enzymatic properties of myosin. It has been reported that the reactivity of the RLR is reduced in the presence of PP_i and nucleotide (*8, 9, 28, 29*). The previous results suggest that the RLR region changes its conformation during ATP hydrolysis. We examined the reac-

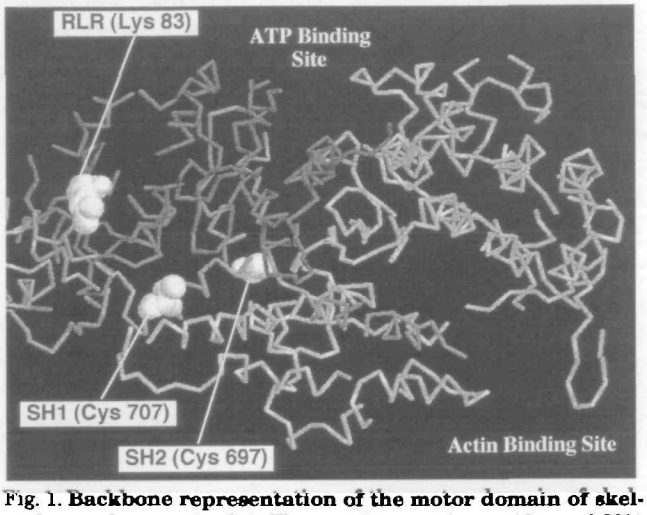

Fig. 1. **Backbone representation of the motor domain of skeletal muscle myosin S-1.** The reactive cysteine residues of SH1 (707), SH2 (697), and the reactive lysine residue RLR (Lys 83) are indicated by their respective space-filling representation. The figure was prepared with the molecular graphic program RasMac 2.7 using the coordinate data (pdb. 2MYS) published by Rayment *et al.* (*3*) in the protein database.

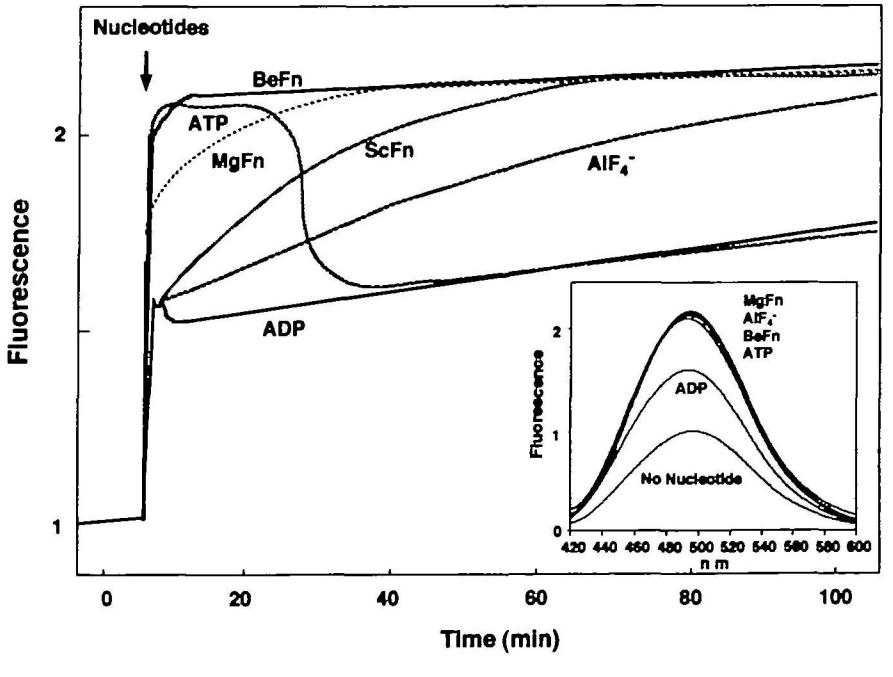

Fig. 2. **To ABD-S-1 (5 μM) in solution with 120 mM NaCl, 30 mM Tris-HCl (pH 7.5), and 2 mM $MgCl_2$, we added 25 μM ATP, 1 mM ADP, 1 mM ADP + 1 mM BeFn, AlF_4^-, or ScFn, or 1 mM ADP + 50 mM NaF at 25°C.** The excitation and emission wavelengths were 390 and 500 nm, respectively. (Inset): Fluorescence spectrum of ABD-S-1·ADP·MgFn ternary complex.

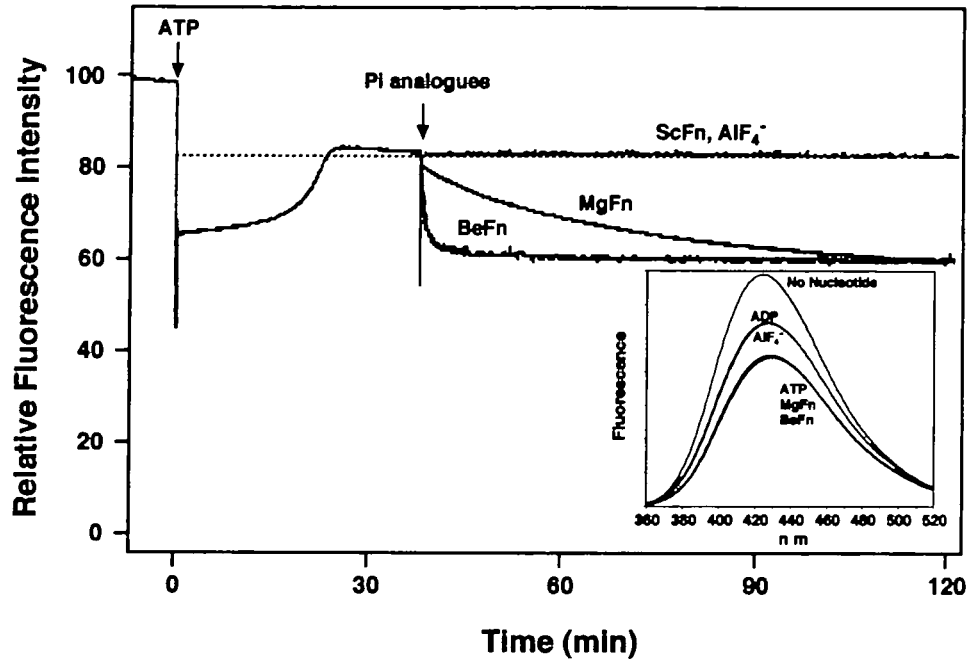

Fig. 3. **Time course of the decrease in MIANS-S-1 fluorescence intensity induced by the formation of the S-1·ADP·MgFn complex.** 6 μM ATP was first added to MIANS-S-1 in 30 mM Tris-HCl, pH 7.5, 120 mM NaCl, 1 μM MIANS-S1, and 5 mM $MgCl_2$. After the complete hydrolysis of ATP, 50 mM NaF was added to the mixture to initiate the formation of the S-1·ADP·MgFn complex. For other ternary complexes, 1 mM BeFn, 1 mM AlF_4^- or 1 mM ScFn were added. The excitation wavelength was 330 nm and emission was monitored at 420 nm. (—) indicates the fluorescent intensity in the presence of ADP. (Inset): Fluorescence spectrum of the MIANS-S-1·ADP·MgFn ternary complex.

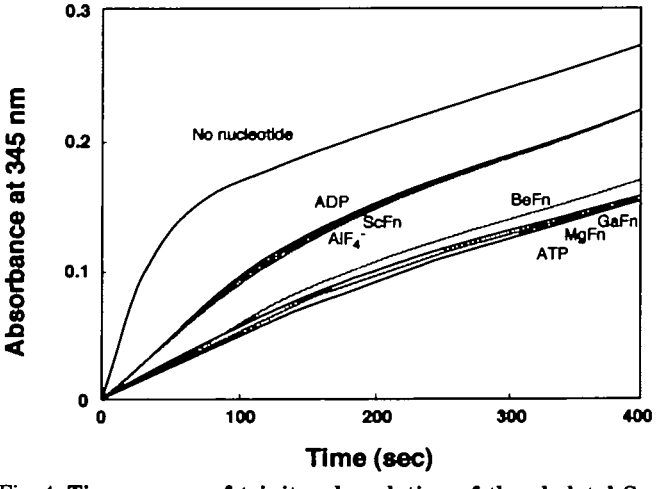

Fig. 4. **Time course of trinitrophenylation of the skeletal S-1·ADP·MgFn complex.** 12 μM S-1 was reacted with trinitrobenzene-sulfonate (0.25 mM) at 25°C in 100 mM imidazole-HCl, pH 7.0, 0.5 M KCl, 5 mM $MgCl_2$, in the presence of 2 mM ATP, 2 mM ADP, 50 mM NaF, 1 mM ADP + 1 mM AlF_4^-, BeFn, ScFn, or 0.1 mM GaFn.

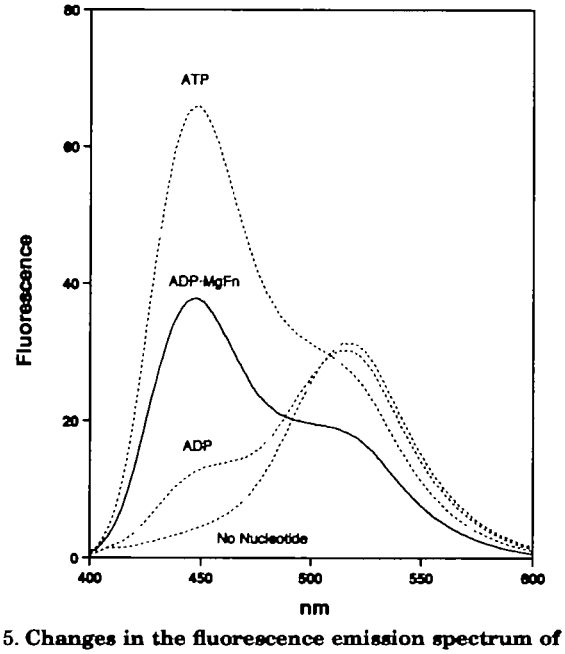

Fig. 5. **Changes in the fluorescence emission spectrum of the prodan·S-1 complex induced by ADP·MgFn.** The fluorescence spectra of the complex of S-1 (20 μM) with prodan (4 μM) were recorded in the presence of 1 mM ADP, 5 mM $MgCl_2$, and 50 mM NaF.

tivity of RLR in the S-1·ADP·MgFn complex and compared it with that seen in the presence of ADP and ATP. As shown in Fig. 4, the rate of trinitrophenylation in the initial phase in the presence of ADP was approximately half of that in the absence of nucleotide, consistent with the results of previous studies (*8*, *9*, *28*, *29*). The addition of ATP completely inhibited trinitrophenylation. ADP and MgFn also completely abolished trinitrophenylation of RLR. This suggests that the conformation at the RLR of the S-1·ADP·MgFn complex resembles that in steady-state ATP hydrolysis. These results suggest that the conformations of the localized regions at SH1, SH2, and RLR on the S-1·ADP·MgFn complex are similar to those of the M^{**}·ADP·P_i state.

Fluorescence Spectra of Prodan·S-1·ADP·MgFn Complex—Hiratsuka (*36*) demonstrated that the noncovalent probe 6-propinyl-2-(dimethylamino)naphthalene (prodan) binds stoichiometrically to S-1 without affecting the ATPase and actin-binding properties S-1. Furthermore, it has been shown that nucleotide-induced changes in prodan fluorescence correspond to the nucleotide-induced conformational states of S-1, suggesting that the fluorescence properties of prodan make it possible to isolate the S-1 in

the M^{**}·ADP·P_i state from the others in the free and S-1^{*}·ADP state. We applied prodan to the study of the conformation of the S-1·ADP·MgFn ternary complex. The fluorescence spectra of the prodan·S-1 complex in the presence of ADP and MgFn were measured according to Hiratsuka (*36*). As shown in Fig. 5, upon the addition of ATP, the fluorescence spectra of prodan·S-1 showed an emission maximum at 445 nm that was accompanied by a marked increase in the fluorescence intensity at 445 nm. In the presence of ADP, the emission maximum was at 450 nm, which was clearly differentiated from that in the presence of ATP as reported previously by Hiratsuka (*36*). Upon the addition of ADP and MgFn, the emission maximum underwent a blue-shift to 445 as seen in the presence of ATP. These results suggest that the formation of the S-1·ADP·MgFn complex is monitored by the fluorescence of prodan. However, the fluorescence intensity of the prodan·S-1·ADP·MgFn complex was approximately twofold lower than that of prodan·S-1 in the presence of ATP. Hiratsuka also reported similar observations for prodan·S-1·ADP·V_i and prodan·S-1·AMP-PNP (*36*). This suggests that the prodan bound to S-1 reflects the differences in conformation of the ATP binding pocket between the S-1·ADP·MgFn complex and S-1^{**}·ADP·P_i.

Small Angle X-Ray Solution Scattering of the S-1·ADP·MgFn Complex—To study the global conformation of the S-1·ADP·MgFn complex, we used a small-angle synchrotron X-ray scattering technique with synchrotron radiation as an intense X-ray source. By measuring the radius of gyration (R_g) from the X-ray scattering curve, Wakabayashi and colleagues (*10*) clearly showed that the myosin head (S-1) changes its shape to a more compact or rounded form in the presence of ATP. They also showed that a similar compaction of the molecule occurs upon the binding of ADP and V_i. The structures of the ternary complexes of S-1·ADP·AlF_4^- and S-1·ADP·BeFn have also been investigated by X-ray scattering. These complexes also have a more compact shape, comparable to that of S-1 in MgATP solution (*18*). We also analyzed the solution structure of the S-1·ADP·MgFn complex by small-angle X-ray scattering and compared it with those of M^{**}·ADP·P_i and other complexes. Figure 6a shows Guinier plots of the scattering data from this complex and those of S-1 in the absence of nucleotide and presence of ATP. The data produced straight lines in the range of $S2 \leq 0.22 \times 10^{-4}$ Å^{-2}, indicating the lack of moleculor aggregates in the solution. The radius of gyration (R_g) was calculated from the slope of the straight lines in the Guinier plots in the range of $0.078 \times 10^{-4} \leq S2 \leq 0.223 \times 10^{-4}$ Å^{-2}, and was plotted against the protein concentration c (Fig. 6b). When extrapolated to $c = 0$, the true R_g value of the S-1·ADP·MgFn complex was about 45.2 Å,

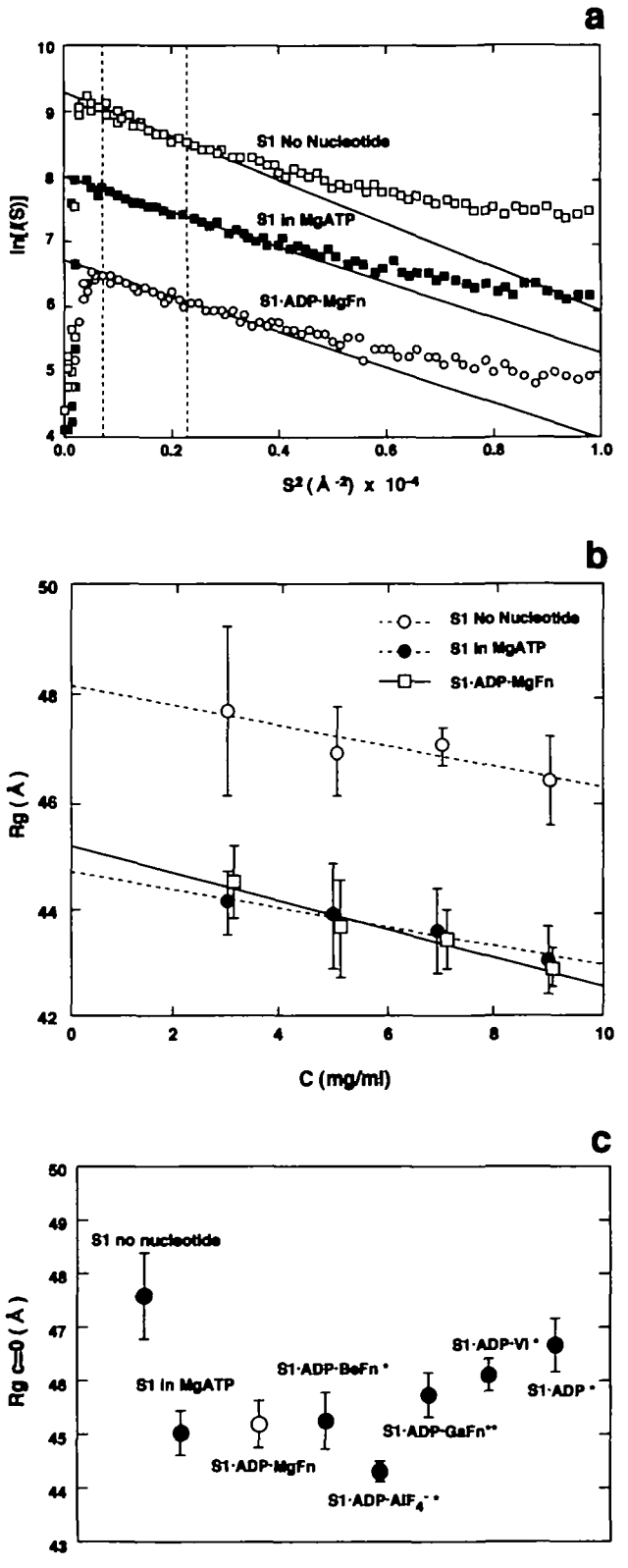

Fig. 6. **(a) Examples of Guinier plots of the small-angle X-ray scattering intensity data from S-1·ADP·MgFn ternary complexes.** Plots of S-1 in the absence of nucleotide and in the presence of ATP are also shown as reference. Data were taken at a concentration of 3.5 mg/ml of S-1·ADP·GaFn and 3.0 mg/ml of S-1 without nucleotide and S1 in the presence of ATP. Vertical lines show the scattering range in which the radius of gyration was calculated from the slope of the straight lines. The three sets of data are shifted vertically for illustrative purposes. **(b) The protein concentration dependence of the radii of gyration (R_g) in samples shown in (a).** ▲, S-1·ADP·MgFn. ○, S-1; ●, S-1 in the presence of ATP. **(c) Comparison of the true R_g values (R_g c = 0) of various S-1 samples.** The true R_gs of the above three samples were obtained by extrapolating the data to zero protein concentration (in Fig. 4a). Data for S-1·ADP·BeFn, S-1·ADP·AlF_4^-, S-1·ADP·V_i and S-1.ADP are those of Sugimoto *et al.* (1995), and marked by single asterisks. Data of S-1·ADP·GaFn, are those of Maruta *et al.* (1999), and marked by double asterisks.

which is clearly less than that in the absence of nucleotide (48 Å) and comparable to that in the presence of MgATP (45 Å) . When compared with the true R_g values of various complexes in Fig. 6c, the value of S-1·ADP·MgFn was smaller than that of S-1·ADP (47 Å), but similar to those of S-1·ADP·BeFn, S-1·ADP·V_i (44.5-46 Å), and slightly larger than that of M**· ADP·P_i (a predominant intermediate state during ATP hydrolysis). Thus, the data clearly demonstrate that the S-1·ADP·MgFn complex is compact or round in shape, similar to M**·ADP·P_i and other complexes with ADP·P_i analogues.

DISCUSSION

Several myosin·ADP·fluorometal (AlF_4^-, BeFn, ScFn, or GaFn) ternary complexes, which mimic transient states in the ATPase cycle, have previously been characterized (*12*, *15*, *16*, *30*). Our previous biochemical experimental data indicated that these complexes are distinct from each other, suggesting that they mimic different transient states along the ATPase cycle. We have proposed a possible order in the alignment of the complexes along the ATPase cycle as BeFn, V_i , ScFn, AlF_4^- along the ATPase cycle in the region from the M*·ATP to the M**·ADP·P_i state (*31*). However, BeFn may mimic the multiple state between the M*·ATP and M**·ADP·P_i state due to some species of BeFn that were observed by ^{19}F-NMR spectrometry (*32*). Indeed, the biochemical experimental data of the S1·ADP·BeFn complex showed the average range of the M*·ATP and M**·ADP·P_i states (*12*). Studying the conformation of the complexes and comparing them with each other may make it possible to determine the sequential conformational changes on the myosin head directly related to energy transduction. The determination of the new ternary complexes mimicking the transient state in the ATPase cycle is important to confirm our approach.

Interestingly, Mg^{2+}, a well known physiological divalent cation, also can form a P_i analogue (MgFn) the same as with Al^{3+} and Be^{2+} in solution. Antonny *et al.* (*33*) demonstrated that MgFn binds to the active site of G-protein with GDP and activates the regulatory protein similar to AlF_4^- and BeFn. Recent crystallographic studies of the myosin motor domain showed structural similarities in the active site to G-protein (*1*, *2*, *17*, *34*, *35*). Such common structural features at the P-loop, switch I, and switch II may be essential for the formation of stable ternary complexes. Recently, Park *et al.* (*19*) showed that myosin also forms a ternary complex with MgFn in the presence of MgADP. They suggested that the S1·ADP·MgFn complex mimics ATPase transients occurring in ATP hydrolysis before phosphate release based on near-ultraviolet circular dichroism, total tryptophan fluorescence, and tryptophan residue 510 quenching measurements. It is interesting to know which transient state steps in the ATPase cycle are mimicked by the S1·ADP·MgFn complex. In the present study, we studied the localized conformation of the ternary complex S1·ADP·MgFn at the region of highly reactive amino acid residues SH1, SH2, and RLR. Such conformational changes directly reflect the formation of a series of transient intermediates during ATP hydrolysis. In particular, the region of the flexible SH1-SH2 residues is thought to act as an energy transduction loop through which intersite communication between the ATP and actin binding sites is transmitted (*26*). As shown in Figs. 2 and 3, the fluorescence intensities of both probes at SH1 and SH2 of the S-1·ADP·MgFn complex were identical to those seen in the presence of ATP. It has been previously shown that labeling by ABDF or MIANS does not affect the formation of ternary complexes of labeled S-1·ADP·AlF_4^- or ScFn (*30*). Moreover, the fluorescence intensity of the MIANS- or ABD-S-1·ADP·MgFn ternary complexes are clearly different from that in the presence of only ADP. Therefore, it seems that ABD-S-1 and MIANS-S-1 form ternary complexes with ADP and MgFn. We have previously demonstrated that SH1 and SH2 move distinctly during ATP hydrolysis and that the local conformations of the SH2 regions more sensitively reflect different transient states (*30*). Actually, the fluorescence of the ABD group bound to SH1 in the ternary complexes of AlF_4^-, BeFn, ScFn, GaFn showed similar intensity. In contrast to SH1, the local conformation at SH2 of the BeFn and GaFn complexes was different from the AlF_4^- and ScFn complexes. Conformational changes at SH2 may not be accompanied by the formation of the M**·ADP·P_i state as is the case with conformational changes at SH1. ATP derivatives of 8-N_3-ATP and 8-Br-ATP, which are hydrolyzed by myosin without formation of the M**·ADP·P_i state, slightly increase the intrinsic tryptophan fluorescence, attenuate MIANS fluorescence at SH2, and dissociate acto-S-1 (*37*). Therefore, local conformational changes at SH2 may be communicated by changes at the actin binding site. Conformational changes in the RLR region are also associated with changes in the SH2 regions. Based on the data shown in Figs. 3 and 4, the conformations at SH2 and RLR of the S-1·ADP·MgFn complex are identical to that of the BeFn complex and differ from those of the AlF_4^- and ScFn complexes, as previously reported (*30*). However, the interaction of the MgFn complex with actin was different from that of the BeFn complex. ADP and BeFn were released by actin more readily than the MgFn complex. Park *et al.* have also shown that the actin-induced dissociation rate of ADP·MgFn and S-1 is about tenfold slower than that of ADP·BeFn and S-1 (*19*). Therefore, the MgFn complex could be clearly differentiated from other complexes. These results support the notion that the respective ternary complexes correspond to analogues of different transient states in the ATPase cycle.

Park *et al.* (*19*) also showed that S1·ADP·MgFn differs from other complexes in quantitative comparison of kinetic and spectroscopic data, and suggested that the structure of S1·ADP·MgFn follows that of S1·ADP·V_i in the ATPase cycle (*19*). Recently, X-ray solution scattering (*10*) demonstrated that the myosin head changes its global conformation during ATP hydrolysis. Analysis of the X-ray scattering data indicated that a conformational change of the myosin head in the presence of ATP is caused by a hinge-like bending motion between the catalytic and regulatory domains (*18*). previously, we used X-ray solution scattering to analyze the structures of S-1·ADP·AlF_4^-, S-1·ADP·BeFn, S-1·ADP·V_i, and S-1·ADP·GaFn, which are thought to be analogues of the M**·ADP·P_i (*16*, *18*). The results indicated that these ternary complexes have a compact or round shape, strongly suggesting that the ternary complexes mimic an intermediate state at or near M**·ADP·P_i in the ATPase cycle. Therefore, we also examined the structure of the S-1·ADP·MgFn complex by X-ray scattering. As expected, the radius of gyration value (R_g) of the S-1·ADP·MgFn complex

(Fig. 6, b and c) was almost identical to that of S1 in the presence of ATP. This finding clearly indicates that the global structure of S-1·ADP·MgFn closely resembles that of the M^{**}·ADP·P_i state. This is consistent with the results of direct observation of the complex using quick freeze deep etch electron microscopy showing a strongly kinked configuration similar to other ternary complexes (Maruta unpublished data).

Park *et al.* (*19*) suggested that the S-1·ADP·MgFn complex resembles ATPase transients occurring during ATP hydrolysis before phosphate release, based on CD spectroscopic analysis, fluorescence enhancement of nucleotide sensitive tryptophan, and acrylamide quenching of Trp 510. However, our experimental data so far suggest that the MgFn complex may mimic an earlier step than that mimicked by the AlF_4^- and ScFn complexes. The localized conformation at SH1, SH2, and RLR of S-1·ADP·MgFn resembles the S-1·ADP·BeFn rather than the AlF_4^- and ScFn complexes. Trp fluorescence enhancement is smaller than that of the AlF_4^- and ScFn complexes. Therefore, we propose that the possible alignment of the S-1·ADP·MgFn ternary complex in the ATPase cycle is between the BeFn and AlF_4^- complexes as follows:

$$\begin{array}{c} \qquad\qquad\quad (\text{ScFn}) \\ {}^{*}\text{BeFn}\ {}^{**}\text{BeFn}\ \text{MgFn}\ AlF_4^- \\ M^{*}\cdot ATP \longrightarrow M^{**}\cdot ADP\cdot P_i \longrightarrow M^{*}\cdot ADP \end{array}$$

(*BeFn and **BeFn indicate different species of MgFn depending on the number of F bound to Be)

The S-1·ADP·BeFn complex mimics the states between M^{*}·ATP and M^{**}·ADP·P_i and has a compact or round shape. Other S-1·ADP·fluorometal complexes, including the MgFn complex, that distribute and mimic at or near the M^{**}·ADP·P_i state are compact or round in global shape but differ slightly from each other with respect to their localized functional regions.

REFERENCES

1. Rayment, I., Rypniewski, W.R., Schmidt-Base, K., Smith, R., Tomchick, D.R., Benning, M.M., Winkelmann, D.A., Weenberg, G., and Holden, H.M. (1993) Three-dimensional structure of myosin subfragment-1: a molecular motor. *Science* **261**, 50–57
2. Fisher, A.J., Smith, C.A., Thoden, J.B., Smith, R., Sutoh, K., Holden, H.M., and Rayment, I. (1995) X-ray structures of the myosin motor domain of *Dictyostelium discoideum* complexed with MgADP·BeFx and MgADP·AlF_4^-. *Biochemistry* **34**, 8960–8972
3. Rayment, I., Holden, H.M., Whittaker, M., Yohn, C.B., Lorenz, M., Holmes, K.C., and Milligan, R.A. (1993) Structure of the actin-myosin complex and its implications for muscle contraction. *Science* **261**, 58–65
4. Werber, M.M., Szent-Gyorgyi, A.G., and Fasman, G.D. (1972) Fluorescence studies on heavy meromyosin-substrate interaction. *Biochemistry* **11**, 2872–2883
5. Harrington, W.F., Reisler, E., and Burke, M. (1975) An activation mechanism for ATP cleavage in muscle. *J. Supramol. Struct.* 112–124
6. Reisler, E., Burke, M. and Harrington, W.F. (1977) Reactivity of essential thiols of myosin. Chemical probes of the activated state. *Biochemistry* **16**, 5187–5191
7. Doung, A. and Reisler, E. (1989) Nucleotide-induced states of myosin subfragment 1 cross-linked to actin. *Biochemistry* **28**, 3502–3509
8. Mornet, D., Pantel, P., Bertrand, R., Audemard, E., and Kassab, R. (1980) Localization of the reactive trinitrophenylated lysyl residue of myosin ATPase site in the NH_2-terminal (27 k domain) of S1 heavy chain. *FEBS Lett.* **117**, 183–188
9. Komatsu, H., Emoto, Y., and Tawada, K. (1993) Half-stoichiometric trinitrophenylation of myosin subfragment 1 in the presence of pyrophosphate or adenosine diphosphate. *J. Biol. Chem.* **268**, 7799–7808
10. Wakabayashi, K., Tokunaga, M., Kohno, I., Sugimoto, Y., Hamanaka, T., Takezawa, Y., Wakabayashi, T., and Amemiya, Y. (1992) Small-angle synchrotron x-ray scattering reveals distinct shape changes of the myosin head during hydrolysis of ATP. *Science* **258**, 443–447
11. Maruta, S., Henry, G.D., Sykes, B.D., and Ikebe, M. (1991) Formation of the stable smooth muscle myosin-ADP-AlF3 complex and its analysis using ^{19}F-NMR. *Biophys. J.* **59**, 436a
12. Maruta, S., Henry, G.D., Sykes, B.D., and Ikebe, M. (1993) Formation of the stable myosin-ADP-aluminum fluoride and myosin-ADP-beryllium fluoride complexes and their analysis using ^{19}F NMR. *J. Biol. Chem.* **268**, 7093–7100
13. Werber, M.M., Peyser, Y.M., and Muhlrad, A. (1992) Characterization of stable beryllium fluoride, aluminum fluoride, and vanadate containing myosin subfragment 1-nucleotide complexes. *Biochemistry* **31**, 7190–7197
14. Phan, B. and Reisler, E. (1992) Inhibition of myosin ATPase by beryllium fluoride. *Biochemistry* **31**, 4787–4793
15. Gopal, D. and Burke, M. (1995) Formation of stable inhibitory complexes of myosin subfragment 1 using fluoroscandium anions. *J. Biol. Chem.* **270**, 19282–19286
16. Maruta, S., Uyehara, Y., Homma, K., Sugimoto, Y., and Wakabayashi, K. (1999) Formation of the myosin·ADP·gallium fluoride complex and its solution structure by small-angle synchrotron X-ray scattering. *J. Biochem.* **125**, 177–185
17. Smith, C.A. and Rayment, I. (1996) X-ray structure of the magnesium(II)·ADP·vanadate complex of the *Dictyostelium discoideum* myosin motor domain to 1.9 Å resolution. *Biochemistry* **35**, 5404–5417
18. Sugimoto, Y., Tokunaga, M., Takezawa, Y., Ikebe, M., and Wakabayashi, K. (1995) Conformational changes of the myosin heads during hydrolysis of ATP as analyzed by x-ray solution scattering. *Biophys. J.* **68**, 29s-34s
19. Park, S., Ajtai, K., and Burghardt, T.P. (1999) Inhibition of myosin ATPase by metal fluoride complexes. *Biochim. Biophys. Acta* **1430**, 127–140
20. Perry, S.V. (1952) Myosin adenosine triphosphatase. *Methods Enzymol.* **2**, 582–588
21. Weeds, A.G. and Taylor, R.S. (1975) Separation of subfragment-1 isoenzymes from rabbit skeletal muscle myosin. *Nature* **257**, 54–56
22. Reisler, E., Burke, M., Himmelfarb, S., and Harrington, W.F. (1974) Spatial proximity of the two essential sulfhydryl groups of myosin. *Biochemistry* **13**, 3837–3840
23. Wells, J.A. and Yount, R.G. (1982) Chemical modification of myosin by active-site trapping of metal-nucleotides with thiol crosslinking reagents. *Methods Enzymol.* **85**, 93–116
24. Cheung, H.C., Gryczynski, I., Malak, H., Wiczk, W., Johnson, M.L., and Lakowicz, J.R. (1991) Conformational flexibility of the Cys 697–Cys 707 segment of myosin subfragment-1. Distance distributions by frequency-domain fluorometry. *Biophys. Chem.* **40**, 1–17
25. Hitatsuka, T. (1992) Movement of Cys-697 in myosin ATPase associated with ATP hydrolysis. *J. Biol. Chem.* **267**, 14941–14948
26. Hiratsuka, T. (1993) Behavior of Cys-707 (SH1) in myosin associated with ATP hydrolysis revealed with a fluorescent probe linked directly to the sulfur atom. *J. Biol. Chem.* **268**, 24742–24750
27. Kubo, S., Tokura, S., and Tonomura, Y (1960) On the active site of myosin A-Adenosine triphosphate. *J. Biol. Chem.* **235**, 2835–2839
28. Miyanishi, T., Inoue, A., and Tonomura, Y. (1979) Differential modification of specific lysine residues in the two kinds of sub-

fragment-1 of myosin with 2,4,6-trinitrobenzenesulfonate. *J. Biochem.* **85**, 747–753
29. Setton, A., and Muhlrad, A. (1988) The effect of pyrophosphate on the reaction of myosin with 2,4,6-trinitrobenzene sulphonate. *J. Muscle Res. Cell Motil.* **9**, 132–146
30. Maruta, S., Homma, K., and Ohki, T. (1998) Conformational changes at the highly reactive cystein and lysine regions of skeletal muscle myosin induced by formation of transition state analogues. *J. Biochem.* **124**, 578–584
31. Homma, K., Uyehara, Y., and Maruta, S. (1998) Myosin-ADP-fluorometal ternary complexes which mimic transient state intermediates along the ATPase cycle. *Biophys. J.* **74**, 260a
32. Henry, G.D., Maruta, S., Ikebe, M., and Sykes, B.D. (1993) Observation of multiple myosin subfragment 1-ADP-fluoroberyllate complexes by 19F NMR spectroscopy. *Biochemistry* **32**, 10451–10456
33. Antonny, B., Sukumar, M., Bigay, J., Chabre, M., and Higashijima, T. (1993) The mechanism of aluminum-independent G-protein activation by fluoride and magnesium. ^{31}P NMR spectroscopy and fluorescence kinetic studies. *J. Biol. Chem.* **268**, 2393–2402
34. Dominguez, R., Freyzon, Y., Trybus, K.M., and Cohen, C. (1998) Crystal structure of a vertebrate smooth muscle myosin motor domain and its complex with the essential light chain: visualization of the pre-power stroke state. *Cell* **94**, 559–571
35. Vale, R.D. (1996) Switches, latches, and amplifiers: common themes of G proteins and molecular motors. *J. Cell Biol.* **35**, 291–302
36. Hiratsuka, T. (1998) Prodan fluorescence reflects differences in nucleotide-induced conformational states in the myosin head and allows continuous visualization of the ATPase reactions. *Biochemistry* **37**, 7167–7176
37. Homma, K. and Maruta, S. (1997) Conformational change at the SH1 and SH2 regions of myosin accompanied by formation of myosin-ATP analogues complexes which mimic the different transient state intermediates along the ATPase cycle. *Biophys. J.* **72**, 181a